Searching for scalar ultralight dark matter via refractive index changes in fibers

J. Manley, R. Stump, R. Petery, and S. Singh[*]

Department of Electrical and Computer Engineering, University of Delaware, Newark, Delaware 19716, USA

We propose using an optical fiber-based interferometer to search for scalar ultralight dark matter (UDM) with particle mass in the range $10^{-17} - 10^{-13}$ eV/c^2 ($10^{-3} - 10$ Hz). Composed of a solid core and a hollow core fiber, the proposed detector would be sensitive to relative oscillations in the fibers' refractive indices due to scalar UDM-induced modulations in the fine-structure constant α. We predict that, implementing detector arrays or cryogenic cooling, the proposed optical fiber-based scalar UDM search has the potential to reach new regions of the parameter space. Such a search would be particularly well-suited to probe for a solar halo of dark matter with a sensitivity exceeding that of previous dark matter searches over the particle mass range $7 \times 10^{-17} - 2 \times 10^{-14}$ eV/c^2.

I. INTRODUCTION

Dark matter (DM) is a substance of unknown composition that accounts for 85% of the matter in the Universe. It is the dominant component of matter in galaxies [1], and its existence is inferred through its gravitational effects on normal matter. The lack of nongravitational observations permits a wide variety of viable DM candidates, along with interactions with Standard Model particles and fields [2,3].

We consider a scalar ultralight dark matter (UDM) scenario, where dark matter is entirely composed of scalar particles with mass $m_{\mathrm{DM}} \lesssim 10$ eV/c^2 that would act as a coherently oscillating scalar field around Earth due to its large number density. Through nongravitational interactions with normal matter, scalar UDM induces an effective oscillation in fundamental constants [4]. Specifically, we consider oscillation of the fine-structure constant α, an effect that can be searched for with a wide variety of detector types [3] including atomic experiments [5–10], optical cavities [11–13], mechanical systems [14,15], and gravitational wave detectors [16–18].

Here we propose a detector that would use optical fibers to search for scalar UDM-induced oscillations in α, which would produce a measurable oscillation of optical refractive indices. Such a detector would probe for UDM by comparing the refractive indices of two different types of

fibers, solid core and hollow core, which would be differentially affected by oscillations in α.

Due to ease of manufacturing coupled with extremely low optical loss, optical fibers are low cost and large channel capacity information transmission devices. These properties make them ubiquitous in long distance classical and quantum communication networks. Technical advances in ultralow loss fibers are being accelerated due to demands in disparate fields such as high-volume online data transmission or quantum cryptography. In a parallel development, photonic crystal fibers offer a novel route to efficiently transmit high
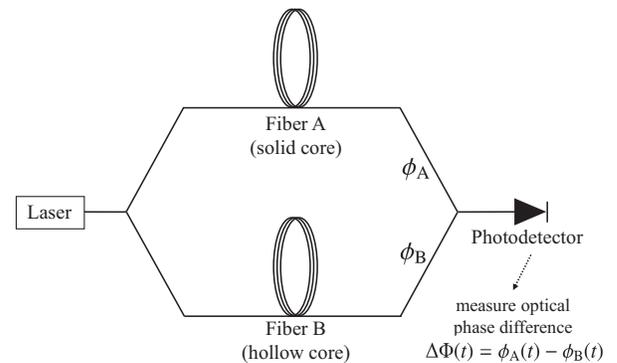
FIG. 1. Conceptual model for an optical fiber-based detector. Relative oscillations in the refractive indices of two fibers can be detected using an optical-path-length-balanced Mach-Zehnder interferometer. Scalar UDM affects the refractive index of the solid core fiber, shifting the optical phase and resulting in an oscillation in output optical power at the UDM frequency. While the noise analysis in this paper assumes a more complex setup (see Fig. 4), which leads to common-mode rejection of various technical noise, the signal can be well-modeled by the setup above.

[*]swatis@udel.edu

power without losses associated with material nonlinearity [19]. When combined with advances in cryogenics fueled by quantum computing, existing and near-term fiber technology offers a promising tabletop route to search for dark matter, achieving sensitivities to scalar UDM that exceed the current constraints over a wide range of sub-Hz frequencies.

This paper is organized as follows: In Sec. II, we provide a brief background of scalar UDM and the signal it produces. In Sec. III, we introduce the concept of an optical fiber-based UDM detector. In Sec. IV we present a model for the noise sources that would limit the detector's sensitivity, and in Sec. V we use this noise model to calculate the minimum detectable coupling strength, which is evaluated considering both Galactic halo and solar halo UDM scenarios. Additional details can be found in the Appendixes, including derivations of expressions in the main text and extended discussion of the noise models used to characterize the prospective UDM detector.

II. SCALAR UDM

For the range of particle masses considered in this work, UDM can be considered a coherent and approximately spatially uniform background field on Earth. This field is nearly monochromatic, oscillating at the Compton frequency $f_{\mathrm{DM}} = m_{\mathrm{DM}} c^2 / h$. Through Doppler broadening, the velocity dispersion of DM gives the field a finite coherence time τ_{DM}. Over timescales less than τ_{DM} the field can be expressed as a sinusoid,

$$\varphi(t) \approx \varphi_0 \cos(2\pi f_{\mathrm{DM}} t + \theta_{\mathrm{DM}}), \tag{1}$$

whose amplitude φ_0 is a stochastic quantity described by a Rayleigh distribution [20]. The field amplitude's root-mean-square value $\varphi_{\mathrm{rms}} = \sqrt{\frac{2 G \rho_{\mathrm{DM}}}{\pi c^2 f_{\mathrm{DM}}^2}}$ is determined by the local dark matter density ρ_{DM}. The values of τ_{DM} and ρ_{DM} depend on the DM halo model being considered. For example, in this work we consider two halo models, (1) a standard, smooth Galactic halo where $\rho_{\mathrm{DM}} \approx 0.4$ GeV/cm³ [1] and $\tau_{\mathrm{DM}} \approx 10^6 \omega_{\mathrm{DM}}^{-1} \approx (1\ \mathrm{Hz}/f_{\mathrm{DM}}) \times 2$ days [21] (see Table I for details), as well as (2) a local UDM halo centered on the Sun, which would have a greater particle density and coherence time (see Sec. V for more details). The unknown phase θ_{DM} has a flat distribution from 0 to 2π [20]. While these temporal and spatial field properties are general to multiple types of UDM, the experimental signature of scalar UDM depends on its specific interactions with Standard Model particles.

We assume scalar UDM couples linearly to the electromagnetic field tensor $F^{\mu\nu}$. Such an interaction is described by the Lagrangian density term [22]

$$\mathcal{L}_{\mathrm{int}} = d_e \varphi(t) \frac{e^2 c}{16 \pi \hbar \alpha_0} F_{\mu\nu} F^{\mu\nu} \tag{2}$$

TABLE I. Quantitative properties of the UDM signal for the particle mass range considered in this work, and key parameters used to calculate the detector's sensitivity. See Table III in Appendix D for more details on the fiber material properties that were used to estimate various noise sources.

Property	Range considered
UDM signal parameters	
Frequency	10^{-3} Hz $\le f_{\mathrm{DM}} \le 10$ Hz
Coherence time	4 hours $\lesssim \tau_{\mathrm{DM}} \lesssim 5$ years
Coherence length	10^7 km $\lesssim \lambda_{\mathrm{DM}} \lesssim 10^{11}$ km
Experiment parameters	
Laser wavelength	$\lambda_{0,\mathrm{L}} = 1550$ nm
Laser power	$P_{\mathrm{L}} = 1$ mW
Length of solid core fiber	$L_{0,\mathrm{A}} = 10$ km
Length of hollow core fiber	$L_{0,\mathrm{B}} = 14.7$ km
Measurement time	$\tau_{\mathrm{int}} = 1$ year

where e is the elementary electric charge, c is the speed of light, $\hbar$ is the reduced Planck constant, and α_0 is the fine-structure constant (in the absence of scalar UDM). The strength of the interaction is parametrized with the dimensionless coupling strength d_e.

Generally, interactions between scalar UDM fields and normal matter can be modeled as variations of fundamental constants [4], such as the electron mass m_e or fine-structure constant α, where the value of a fundamental constant at any point in space or time depends on the local value of the scalar UDM field. In the case of Eq. (2), scalar UDM causes fractional fluctuations in the fine-structure constant given by

$$\frac{\delta\alpha}{\alpha_0}(t) = d_e \varphi(t). \tag{3}$$

Oscillations in α produce measurable effects such as modulation of atomic energy levels [14], material refractive indices [23], and mechanical strains [24,25].

Scalar UDM-induced oscillations in the fine-structure constant lead to a material-dependent oscillation of optical refractive indices, and the proposed fiber-based detector would be sensitive to scalar UDM primarily through its modulation of an optical fiber's refractive index. The refractive index of an optical material generally depends on the fine-structure constant [23,26]. For small fluctuations in α, the resulting fractional fluctuation in refractive index is

$$\frac{\delta n}{n_0} = \epsilon_{n\alpha} \frac{\delta\alpha}{\alpha_0}, \tag{4}$$

where $\epsilon_{n\alpha} \equiv \frac{\alpha_0}{n_0} \frac{\partial n}{\partial \alpha} |_{\alpha=\alpha_0}$. While the coefficient $\epsilon_{n\alpha}$ may not be directly measurable, it can be related to a material's optical dispersion as [23,26]

$$\epsilon_{n\alpha} = -2\epsilon_{n\omega_{\mathrm{L}}}, \tag{5}$$

where $\epsilon_{n\omega_{\mathrm{L}}} \equiv \frac{\omega_{\mathrm{L}}}{n_0} \frac{\partial n}{\partial \omega_{\mathrm{L}}}|_{\omega_{\mathrm{L}}=\omega_{0,\mathrm{L}}}$, ω_{L} is the optical angular frequency, and $\omega_{0,\mathrm{L}}$ is the angular frequency of the laser. Details of the model used to derive Eq. (5) are given in Appendix B.

III. OPTICAL FIBERS AS DM DETECTORS

Here we propose to search for scalar UDM by comparing the refractive indices of two different types of fibers, solid core and hollow core fibers, which are differentially affected by oscillations in the fine-structure constant. In solid core fibers, the optical mode is contained within silica ($n_A \approx n_{\mathrm{silica}} \approx 1.5$), for which $\epsilon_{n\omega_{\mathrm{L}},\mathrm{silica}} = 0.013$ at an optical wavelength of 1550 nm (see Appendix B). In hollow core fibers, the optical mode is mostly contained within air (or vacuum) ($n_B \approx n_{\mathrm{air}} \approx 1$ [27]), for which $\epsilon_{n\omega_{\mathrm{L}},\mathrm{air}} \ll \epsilon_{n\omega_{\mathrm{L}},\mathrm{silica}}$ [28,29].

A simple model for a fiber-based scalar UDM detector is an optical-path-length-balanced Mach-Zehnder interferometer, as depicted in Fig. 1, where a solid core fiber and a hollow core fiber each constitute an interferometer arm. By balancing the optical path lengths of each fiber, some common mode noise sources can be suppressed, and oscillations in the relative optical lengths of the fibers can be measured interferometrically using a laser with central wavelength $\lambda_{0,\mathrm{L}} = 1550$ nm and average power ~1 mW. Small fluctuations in α due to scalar UDM result in a phase difference signal with magnitude

$$\Delta\Phi^{\mathrm{DM}} = \omega_{0,\mathrm{L}}\tau_0\epsilon_{n\omega_{\mathrm{L}},\mathrm{silica}}\frac{\delta\alpha}{\alpha_0}, \qquad (6)$$

where $\tau_0 = n_0 L_0/c$ is the time delay. A detailed derivation of the output phase difference, including the UDM-induced phase difference given in Eq. (6), is given in Appendix C.

Appendix C also introduces a modified version of the interferometric setup (see Fig. 1), which enables the cancellation of several phase noise sources. As detailed derivations in Appendixes C and D 1 show, the detector geometry displayed in Fig. 4 has a sensitivity that is consistent with a balanced interferometer (represented in Fig. 1), while being immune to laser frequency noise. We note that the quantitative results presented below in Figs. 2 and 3 are for the setup shown in Fig. 4.

Scalar UDM also produces a strain signal [24,25] that affects the experiment via a coherent oscillation in the lengths of the fibers and the laser cavity. Because both fibers are primarily composed of the same materials, the strain is common to both interferometer arms and does not produce a measurable phase difference (also, the material dependence of the strain would be a higher-order effect [31]). However, straining the laser cavity shifts the laser's central wavelength, producing an optical path length imbalance due to differences of optical dispersion
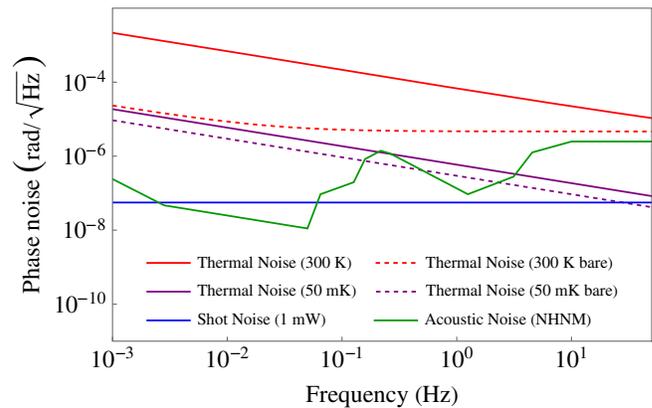
FIG. 2. Estimated phase noise for the fiber-based detector. Contributions are included from each of the noise sources detailed in Sec. IV. Several thermal noise curves are included, corresponding to fibers with (solid lines) and without (dashed lines) polymer coatings at temperatures of 300 K and 50 mK.

between the fibers. Therefore, while the presence of scalar UDM would ultimately be inferred from relative oscillations in the fibers' refractive indices, it is worth noting that this signal includes contributions from both direct modulation of the solid core fiber's refractive index as well as the strain in the laser cavity (via optical dispersion in the fibers). Incidentally, for the case of scalar UDM coupling to the electron mass, this effect cancels the signal produced through direct refractive index modulation of the fibers (see Appendix B). For this reason, the detector is only sensitive to oscillations in the fine-structure constant. We note that a different combination of fiber-based interferometry and laser stabilization might enable measurement of a differential length change effect, or access to the electron mass coupling to UDM. More importantly, our analysis highlights the importance of including the effect of the omnipresent UDM signal on the experimental apparatus beyond the interferometer.

IV. NOISE

Various noise sources have the potential to overshadow the DM signal $\Delta\Phi^{\mathrm{DM}}$. The dominant noise sources to be considered when designing a fiber-based UDM detector are thermal noise and acoustic noise in the fibers themselves, noise from the laser, and photon shot noise. The effect of each noise source is quantified by a one-sided phase noise power spectral density (PSD) $S_{\Delta\Phi}(f)$, and plotted in Fig. 2.

Thermomechanical noise in the fibers will likely set the ultimate limit to the detector's sensitivity. Fiber "thermomechanical noise" $S_{\delta\phi}^{\mathrm{TM}}$ refers to the optical phase fluctuations $\delta\phi$ that are induced by spontaneous thermal fluctuations of a fiber's length due to internal friction [32]. The fluctuation-dissipation theorem provides an
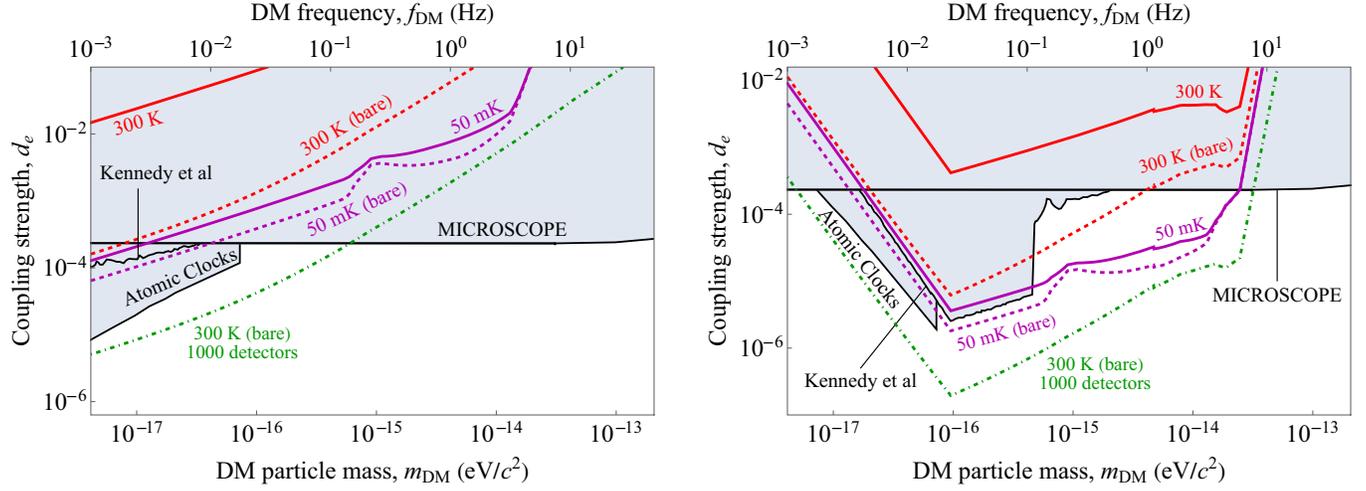
FIG. 3.   Projected constraints on d_e from optical fibers, for Galactic (left) and solar (right) DM halos. Curves are included for fiber detectors operating at temperatures of 300 K and 50 mK, with (solid) and without (dashed) polymer coatings, for a measurement time $\tau_{exp} = 1$ year. The fiber lengths are chosen to be $L_{0,A} = 10$ km and $L_{0,B} \approx 15$ km. The detectors are primarily limited by thermal noise; cryogenic detectors start to become limited by acoustic noise at frequencies above $\sim 10^{-1}$ Hz. Also included are projected constraints from an array of 1000 detectors, using bare fiber at room temperature. The strongest experimental constraints in this mass range come from MICROSCOPE [30], Kennedy *et al.* [12], and atomic clock comparisons (here included as a rough, combined constraint from Filzinger *et al.* [8] and Sherrill *et al.* [9]).

accurate model for thermomechanical noise in fibers, resulting in a phase noise PSD given by [33]

$$S_{\delta\phi,i}^{TM}(f) = \left(\frac{2\pi n_{0,i}}{\lambda_{0,L}}\right)^2 \frac{2k_B T L_{0,i}\xi_i}{3\pi E_i A_i}\frac{1}{f}, \qquad (7)$$

where T is the temperature, $L_{0,i}$ is the physical length, ξ_i is the mechanical loss tangent, E_i is the Young's modulus, and A_i is the cross sectional area of fiber i. The resulting differential phase noise in the interferometer is the sum of contributions from both fibers A and B: $S_{\Delta\Phi}^{TM} = S_{\delta\phi,A}^{TM} + S_{\delta\phi,B}^{TM}$. Several experiments have directly measured thermomechanical noise in single mode fibers [34,35], and the thermomechanical noise model described by Eq. (7) has been verified down to frequencies as low as 0.05 Hz [36]. In Figs. 2 and 3 we extend this model down to 1 mHz to explore the possible low-frequency performance of a fiber-based detector under the assumption that low-frequency technical noise sources such as thermal drift or laser intensity fluctuations are adequately suppressed.

As a method for reducing thermomechanical noise we propose reducing the thickness of the fibers' polymer coatings. Mechanical loss in fibers likely comes primarily from the polymer coatings that protect the silica cladding, and there is some evidence suggesting that reducing the thickness of these coatings reduces the thermomechanical noise floor in optical fibers [35]. We include thermal noise estimates in Fig. 2 for bare (without coating) fibers as a benchmark approximation for thinly coated fibers, noting that while fiber coatings can be made quite thin [27], bare

fibers may be difficult to manufacture and handle due to fragility. Appendix D 3 has a detailed discussion of mechanical dissipation in optical fibers, including the values of the parameters used in the thermal noise estimates for Fig. 2.

Another way to reduce thermal noise is to implement cryogenic cooling. Figure 2 illustrates the impact on thermal noise of lowering the temperature from room temperature (300 K) to cryogenic temperature (50 mK). It is clear from the figure that the benefit of removing the coatings diminishes at lower temperature, where the intrinsic mechanical loss tangent ξ of fused silica increases beyond its room-temperature value.

To achieve a thermally limited detection sensitivity, steps need to be taken to shield the experiment from acoustic noise in the fibers. Mechanical vibrations, which may originate from a variety of sources such as human activity, natural seismic activity, or local weather, often pose a challenge for terrestrial experiments at low frequencies. Vibration-induced strains in optical fibers can be suppressed by using low vibration sensitivity fiber spools [37] and by cowinding the fibers on the same spool to correlate the acoustic noise between them [34,35]. The remaining effects then come from differences in the strain optic effect between the two fibers (see Appendix D 4 for more details). To estimate the effects of mechanical vibrations, we use the United States Geological Survey New High Noise Model (NHNM) for seismic noise [38]. By cowinding both fibers on a single vibration-insensitive spool, acoustic noise at the level predicted by the NHNM can be reduced to a level comparable to that of thermal noise in this experiment, as can be seen in Fig. 2.

The final noise source included in Fig. 2 is photon shot noise, which can be limited to a subdominant level by ensuring sufficient output optical power despite propagation losses in the fibers. Recent advances in hollow core fiber technology have yielded hollow core fibers with a propagation loss of 0.17 dB/km at $\lambda_{0,\mathrm{L}} = 1550$ nm [39], reaching the level of low-loss solid core fibers (0.18 dB/km for SMF28 [40]). We find that shot noise in this experiment can be limited to below the thermal noise floor at cryogenic temperatures with an input laser power of $P_{\mathrm{L}} \sim 1$ mW (see Appendix D 2 for more details). The laser shot noise can be further reduced by employing quantum optical techniques such as squeezing.

A more detailed discussion of these noise sources can be found in Appendix D, along with discussion of techniques to address frequency and intensity noise in the laser. In addition, Ref. [41] also has a comprehensive review on the noise performance of optical fibers in interferometric setups for precision measurements.

V. MINIMUM DETECTABLE COUPLING STRENGTH

The smallest signal a detector is capable of measuring can be inferred from the modeled noise floor, and is improved upon by increasing the duration of the measurement $\tau_{\exp}$. Here, the minimum detectable signal strength $\Delta\Phi_{\min}^{\mathrm{DM}}$ is defined as the signal strength needed to achieve a unity signal to noise ratio. For measurement times less than the DM coherence time ($\tau_{\exp} \lesssim \tau_{\mathrm{DM}}$), the signal can be considered coherent and stochastic, such that $\Delta\Phi_{\min}^{\mathrm{DM}} \propto 3\tau_{\exp}^{-1/2}$ [20]. For significantly longer measurement times ($\tau_{\exp} \gg \tau_{\mathrm{DM}}$), $\Delta\Phi_{\min}^{\mathrm{DM}} \propto (\tau_{\mathrm{DM}}\tau_{\exp})^{-1/4}$ [42]. Here, we combine both regimes into a single smooth function (see Appendix E for more details) to approximate the minimum detectable signal:

$$\Delta\Phi_{\min}^{\mathrm{DM}} \approx \sqrt{2S_{\Delta\Phi}^{\mathrm{noise}}}[3\tau_{\exp}^{-1/2} + (\tau_{\mathrm{DM}}\tau_{\exp})^{-1/4}]. \quad (8)$$

The utility of a potential UDM experiment is typically evaluated by its projected minimum detectable coupling strength $d_{e,\min}$, a quantity that depends on the astrophysical DM model being considered. The minimum detectable coupling strength $d_{e,\min}$ for the detector can be related to the signal strength via Eq. (6) as

$$d_{e,\min} = \frac{\Delta\Phi_{\min}^{\mathrm{DM}}}{\omega_{0,\mathrm{L}}\tau_0\epsilon_{n\omega_{\mathrm{L}},\mathrm{silica}}\varphi_{\mathrm{rms}}}. \quad (9)$$

The minimum detectable coupling strength $d_{e,\min}$ depends on the local energy density ρ_{DM} and coherence time τ_{DM} of the DM; here we consider two different astrophysical DM models for these parameters. The spatial distribution of dark matter across the Milky Way is typically estimated with the Standard Halo Model, which assumes a gravitationally stable and spherically symmetric density profile that decreases with distance from the center of the Galaxy $\rho_{\mathrm{DM}}(r) \propto r^{-2}$ and a Maxwellian velocity distribution [1].

The most commonly used model for UDM in direct detection experiments assumes a smooth Galactic halo, lacking any noticeable substructure, where the DM density and coherence time at Earth take on values determined by the average density and velocity dispersion within the solar neighborhood: $\rho_{\mathrm{DM}} \approx 0.4$ GeV/cm^3 [1] and $\tau_{\mathrm{DM}} \approx 10^6\omega_{\mathrm{DM}}^{-1}$ [21]. The projected constraints from optical fibers, using a Galactic halo model for DM, are plotted in Fig. 3 (left).

We also consider an alternative UDM model, where it is assumed that UDM forms a local halo centered on the Sun [43]. It is possible that DM forms gravitationally bounded objects, which could potentially form a halo bound to an external gravitational source, such as the Sun or Earth [43], while maintaining consistency with the Standard Halo Model on larger scales. In this scenario, the local DM halo could have a greater density and coherence time at Earth than in the Galactic halo model, leading to potentially stronger constraints on coupling strength from direct detection experiments. The halo's size and density would generally depend on the mass of the DM particles. Earth halos are well-motivated at particle energies 10^{-13} eV $\lesssim m_{\mathrm{DM}}c^2 \lesssim 10^{-7}$ eV [43], and several recent experiments have set constraints on the Earth halo model for DM [13,17,44–46]. A fiber-based detector is aptly suited to search for a local DM halo that is gravitationally bound to the Sun, as such solar halos are well-motivated in the particle energy range 10^{-17} eV $\lesssim m_{\mathrm{DM}}c^2 \lesssim 10^{-13}$ eV [43]. In this range, a solar halo could have an energy density up to $\sim 10^5$ times greater than that of a Galactic halo. The projected constraints from optical fibers, using a solar halo model for DM, are plotted in Fig. 3 (right). To recalculate $d_{e,\min}$ for a solar DM halo, we rescale ρ_{DM} using Supplementary Figure 2 from Ref. [43] and use $\tau_{\mathrm{DM}} = 10^8$ s$(\frac{1\,\mathrm{Hz}}{f_{\mathrm{DM}}})^3$ [47]. Constraints on both halo models can be calculated on the same data acquired in a single experimental run, so long as the difference in the expected coherence times is accounted for in the postprocessing.

The parameter space for scalar UDM is plotted in Fig. 3 for both Galactic (left) and solar (right) DM halos. The allowable parameter space is constrained by previous experiments, including both DM direct detection experiments and DM-independent equivalence principle (EP) tests. Experiments designed to test the equivalence principle [30,48] set constraints on scalar interactions regardless of whether the scalar field composes DM. The strongest EP-test constraints in this mass range come from MICROSCOPE [30], which has constrained $d_e \lesssim 10^{-4}$ for $m_{\mathrm{DM}} \lesssim 10^{-13}$ eV/c^2. This constraint does not depend on the DM energy density ρ_{DM}, so it applies equally to both

halo models in Fig. 3. Also included are constraints from the DM direct detection experiments in Refs. [8,9,12], which depend on the DM halo model considered.

The potential of fiber-based scalar UDM detectors operating for $\tau_{\mathrm{exp}} = 1$ year can be seen in Fig. 3, where projections for $d_{e,\mathrm{min}}$ are plotted for various experimental parameters. Fiber-based detectors operating at room temperature and 50 mK, with and without polymer coatings, are considered to search for DM in the particle energy range 10^{-17} eV $\lesssim m_{\mathrm{DM}}c^2 \lesssim 10^{-13}$ eV (10^{-3} Hz $\lesssim f_{\mathrm{DM}} \lesssim 10$ Hz).

To enable room-temperature optical fibers to set more competitive constraints on d_e, an array of N detectors can be implemented for background rejection and averaging down the effects of stochastic noise sources. The UDM coherence length $\lambda_{\mathrm{c}} \approx (1 \text{ Hz}/f_{\mathrm{DM}}) \times 10^7$ km [21] is greater than 10^6 km for frequencies below 10 Hz, allowing for coherent averaging of the signals collected by sites anywhere on Earth to improve the sensitivity as $N^{-1/2}$ [49]. To achieve a significant improvement over the current constraints on d_e for a standard Galactic halo UDM model, a network of around $N \sim 1000$ would be needed. The expected constraints from an array of 1000 detectors with bare fibers at room temperature are included in green. While we acknowledge the logistical challenges associated with launching and maintaining such a network, the technology involved in such detectors already exists and can be mass produced.

VI. SUMMARY AND OUTLOOK

In summary, we have investigated optical fibers as detectors for scalar ultralight dark matter. Dark matter-induced oscillations in the fine-structure constant α would produce a potentially measurable oscillation in fibers' optical path lengths that could be detected in a fiber-based interferometer. To estimate the detection capabilities of optical fibers, we propose an idea for a detector that could measure oscillations in the relative refractive indices of two different types of fibers that are differentially affected by scalar UDM. Accounting for various noise sources, we calculated the minimum detectable scalar UDM coupling strength considering two different UDM models (Galactic and solar halos), finding that cryogenically cooled fiber-based detectors can achieve sensitivities to scalar UDM that exceed the current constraints at sub-Hz frequencies.

In addition to cryogenic cooling, competitive sensitivities can be achieved by using longer fibers or selecting (or fabricating) a better choice of optical fiber. The ideal fiber would likely have a thicker cladding and lower mechanical loss to reduce thermomechanical noise, and low optical loss to reduce shot noise and photothermal heating effects. Finally, the compactness of optical fibers facilitates array-based detection, where a network of detectors can be deployed to improve the overall sensitivity as well as to probe for local substructure in the UDM field.

Optical fibers are a mature technology with a multitude of applications in classical and quantum communication. Increasingly low tolerance for optical loss is driving various technological developments, making them a viable candidate for precision measurements beyond those relying on low photon number quantum optical effects. Creative ideas to harness such technology to study fundamental science are already emerging, such as those involving optical clock networks [50,51]. Along with using fibers as delay lines [13] to look for scalar UDM or as a waveguide to search for axions [52], our proposed interferometric scheme demonstrates that existing optical fiber technology can be repurposed to search for ultralight dark matter. Taken together, these developments present a promising avenue to harness this widely used technology in the search for beyond the Standard Model physics.

APPENDIX A: DEFINITIONS AND MODEL ASSUMPTIONS

Assumption 1: We restrict our analysis to low frequencies, defined by $f_{\mathrm{DM}} \ll \tau_{0,i}^{-1}$; i.e. this derivation holds when the DM Compton frequency is significantly below the inverse time delay of both fibers.

Assumption 2: All fluctuations are small:

$$\left\{ \frac{\delta x}{x_0}, \frac{\delta L_i}{L_{0,i}}, \frac{\delta n_i}{n_{0,i}}, \frac{\delta \omega_{\mathrm{L}}}{\omega_{0,\mathrm{L}}} \right\} \ll 1.$$

Definition of ϵ coefficients: Consider a quantity $w(v)$ with steady-state value $w_0 \equiv w(v_0)$ determined by the steady-state value of its parameter v_0. Assuming small fluctuations ($\delta v \ll v_0$) in v about v_0, the fractional fluctuations of w can be expressed to first order as

$$\frac{\delta w}{w_0} \approx \epsilon_{wv} \frac{\delta v}{v_0},$$

where

$$\epsilon_{wv} \equiv \frac{v_0}{w_0} \frac{\partial w}{\partial v}\bigg|_{v=v_0}. \qquad (A1)$$

Note that while ϵ_{wv} is dimensionless and resembles the sensitivity coefficients discussed in Ref. [53], the ϵ

coefficients used in this work will not generally be independent in the choice of units. We use SI units throughout. We also define the quantities $\Delta\epsilon_{wv} \equiv \epsilon_{wv,\mathrm{A}} - \epsilon_{wv,\mathrm{B}}$.

APPENDIX B: DM COUPLING TO REFRACTIVE INDEX

The dependence of a dielectric medium's refractive index on fundamental constants such as α and m_e can be estimated using a Lorentz model, which assumes that the medium is a collection of resonant atoms responding harmonically to an applied electric field. The refractive index depends on the electric susceptibility $n^2 = \chi + 1$, which accounts for multiple electron and phonon modes by considering the sum over all modes, $\chi = \sum_k \chi_k$. The susceptibility of each mode takes the following form off resonance [23]:

$$\chi_k = 4\pi\hbar c\alpha \frac{N_k}{M_k} \frac{f_k}{\omega_k^2 - \omega^2}. \tag{B1}$$

Here, N_k is the effective number density, M_k is the reduced effective mass, f_k is the oscillator strength, and ω_k is the resonance frequency. The number density is inversely proportional to the atomic/molecular volume [determined by the Bohr radius $a_\mathrm{B} \propto (\alpha m_e)^{-1}$], such that $N_k \propto (\alpha m_e)^3$. For electron modes, $M_k = m_e$; for phonon modes, M_k is independent of α, m_e, and ω [23]. The oscillator strengths f_k are also approximately independent of α, m_e, and ω [23]. For both electron and phonon modes, it can be shown that

$$\chi_k \propto (1 - \omega^2\omega_k^{-2})^{-1}. \tag{B2}$$

Therefore, the dependence on fundamental constants α and m_e is entirely accounted for by the resonance frequencies ω_k. For phonon modes $\omega_k \propto m_e^{3/2}\alpha^2$; for electron modes $\omega_k \propto m_e\alpha^2$ [23].

If the laser frequency is assumed to be in a range where it is reasonable to consider either only phonon modes or only electron modes (i.e. relationship between ω_k and the

TABLE II. Summary of fluctuations included in the derivation of $\Delta\Phi_\mathrm{A}$, due to both noise and DM. Each effect is expressed as a fluctuation in length, refractive index, or simply optical phase.

Effect	Expression
DM-index coupling	$\frac{\delta n_i}{n_{0,i}} = \epsilon_{nx,i}\frac{\delta x}{x_0}$
DM-length coupling	$\frac{\delta L_i}{L_{0,i}} = \epsilon_{Lx,i}\frac{\delta x}{x_0}$
Mechanical vibrations	$\frac{\delta L_i}{L_{0,i}} = h_i^{\mathrm{acoustic}}$
Vibrations (strain-optic)	$\frac{\delta n_i}{n_{0,i}} = \epsilon_{nL,i}h_i^{\mathrm{acoustic}}$
Optical dispersion	$\frac{\delta n_i}{n_{0,i}} = \epsilon_{n\omega_\mathrm{L},i}\frac{\delta\omega_\mathrm{L}}{\omega_{0,\mathrm{L}}}$
Fiber thermal noise	$\delta\phi_i = \delta\phi_i^{\mathrm{thermal}}$
Shot noise (at detector)	$\delta\phi_i = \delta\phi_i^{\mathrm{shot}}$

fundamental constants is independent of mode number k), Eq. (B1) implies that

$$\frac{x}{n}\frac{\partial n}{\partial x} = -\left(\frac{x}{\omega_k}\frac{\partial\omega_k}{\partial x}\right)\left(\frac{\omega}{n}\frac{\partial n}{\partial\omega}\right) \tag{B3}$$

where $x \in \{\alpha, m_e\}$. Equation (B2) allows one to calculate the response of a material's refractive index to variations of fundamental constants using the material's dispersion, which can be measured experimentally.

For variations in α,

$$\frac{\alpha}{n}\frac{\partial n}{\partial\alpha} = -2\left(\frac{\omega}{n}\frac{\partial n}{\partial\omega}\right), \tag{B4}$$

regardless of the type of mode. However, the refractive index's dependence on m_e depends on which modes dominate:

$$\frac{m_e}{n}\frac{\partial n}{\partial m_e} = \begin{cases} -\left(\frac{\omega}{n}\frac{\partial n}{\partial\omega}\right) & \text{electron modes} \\ -\frac{3}{2}\left(\frac{\omega}{n}\frac{\partial n}{\partial\omega}\right) & \text{phonon modes.} \end{cases} \tag{B5}$$

Following Ref. [26], it is assumed that electron modes dominate the dispersion of fused silica, in which case

$$\epsilon_{n\alpha,\mathrm{silica}} = -2\epsilon_{n\omega_\mathrm{L},\mathrm{silica}} \tag{B6}$$

$$\epsilon_{nm_e,\mathrm{silica}} = -\epsilon_{n\omega_\mathrm{L},\mathrm{silica}}. \tag{B7}$$

From the three-term Sellmeier equation for fused silica [54], $\epsilon_{n\omega_\mathrm{L},\mathrm{silica}} = 0.013$. Since the optical dispersion and, therefore, DM coupling to the refractive index of air, are significantly less than that of silica, it is assumed that $\{\epsilon_{nx,\mathrm{air}}, \epsilon_{n\omega_\mathrm{L},\mathrm{air}}\} = 0$.

The DM signal [Eq. (C4)] is proportional to $\epsilon_{nx,\mathrm{silica}} + \epsilon_{n\omega_\mathrm{L},\mathrm{silica}}$. Evidently, from Eqs. (B5) and (B6), the detector is only sensitive to DM-induced oscillations in α, not m_e, since $\epsilon_{nm_e,\mathrm{silica}} + \epsilon_{n\omega_\mathrm{L},\mathrm{silica}} = (-\epsilon_{n\omega_\mathrm{L},\mathrm{silica}}) + \epsilon_{n\omega_\mathrm{L},\mathrm{silica}} = 0$. We note that a more detailed analysis (beyond the simple Lorentz model used here) of the refractive index of silica may affect this result.

APPENDIX C: DERIVATION OF OUTPUT PHASE DIFFERENCE $\Delta\Phi_\mathrm{A}$

In this section we derive an expression for the output phase difference $\Delta\Phi_\mathrm{A}$ for the detector displayed in Fig. 4 in terms of fluctuations due to both noise and the dark matter signal.

This analysis is general to the DM-modulation of both electron mass m_e and the fine-structure constant α; fundamental constants will be generally represented by the variable $x \in \{m_e, \alpha\}$. While it was shown in Appendix A that for our specific choice of detector configuration and the model for refractive index, the detector is not sensitive to oscillation in m_e, a different material choice and/or

FIG. 4. Detector model with FDL-stabilized laser: The purpose of this detector geometry is to eliminate the effects of laser phase noise relative to the geometry proposed in Fig. 1. Fiber B serves as a delay line in an interferometer to stabilize a tunable laser. Using feedback from the measurement at Photodetector B (PD B), the laser frequency is tuned such that $\Delta\Phi_B$ remains constant. The phase difference $\Delta\Phi_A$ would then contain the DM signal. The phase difference $\Delta\Phi_A$ depends linearly on the optical power when the recombining beams are kept near quadrature bias ($\Delta\Phi_A$ mod $2\pi = \pi/2$). In the presence of noise and long term instabilities, quadrature bias can be maintained by including a phase modulator (PM) that is driven by feedback from Photodetector A (PD A). The DM signal is then present in the feedback signal supplied to the phase modulator.

configuration might give access to the d_{m_e} coupling. The analysis presented here can be applied to other material-based interferometer schemes with minimal modifications.

For simplicity, we introduced the detector as a simple optical-length-balanced interferometer in the main text (see Fig. 1). In order to cancel the detrimental effects of a variety of technical noise sources, we now assume a more complex geometry as shown in Fig. 4. Our detailed analysis in this and the next section will reveal that several technical noise sources can be suppressed via common-mode rejection in this, more complex, configuration. In essence, the detector geometry displayed in Fig. 4 has a sensitivity that is consistent with a balanced interferometer (represented in Fig. 1), while being immune to laser frequency noise. We note that the quantitative results presented in Figs. 2 and 3 come from the derivations presented here, which assume the experimental geometry of Fig. 4.

1. Fractional fluctuations of fiber refractive index and length

Fiber i's refractive index $n_i(x, \omega_L)$ depends on the fundamental constant x, the laser frequency ω_L due to optical dispersion, and vibration-induced strains h_i^{acoustic} via the strain-optic effect:

$$\frac{\delta n_i}{n_{0,i}} = \epsilon_{nx,i}\frac{\delta x}{x_0} + \epsilon_{n\omega_L,i}\frac{\delta\omega_L}{\omega_{0,L}} + \epsilon_{nL,i}h_i^{\text{acoustic}}. \quad \text{(C1)}$$

Additionally, the fiber lengths depend on fundamental constant x, as the length of a solid is proportional to the Bohr radius, which will be affected by fluctuations in m_e or α ($a_B \propto (m_e\alpha)^{-1}$) [24,25]. Since $\epsilon_{Lx,i} = -1$ for both fibers, the differential scheme described in Fig. 1 is insensitive to this strain signal.

2. Optical phase at fiber output

Consider a simple fiber interferometer as depicted in Fig. 5. If the phase of light entering a fiber is $\phi_L(t)$, then the phase of light exiting the fiber will be equal to the input phase at an earlier time $\phi_i(t) = \phi_L(t - \tau_i(t))$, where τ_i is the time it takes for an optical wavefront to traverse the entire length of the fiber. In the low-frequency limit (Assumption 1) the time delay is simply related to the fiber's instantaneous optical path length $\tau_i(t) = n_i(t)L_i(t)/c$, and the output phase is

$$\phi_i(t) = \phi_L(t) - \omega_L(t)n_i(t)L_i(t)/c.$$

Including small fluctuations of the optical frequency, fiber index, and fiber length, the output optical phase can be written as

$$\phi_i \approx \phi_L - \omega_{0,L}\tau_{0,i}\left(1 + \frac{\delta n_i}{n_{0,i}} + \frac{\delta L_i}{L_{0,i}} + \frac{\delta\omega_L}{\omega_{0,L}}\right).$$

We have omitted from our notation the explicit time dependence of each variable (t), since the analysis considers the quasistatic (low-frequency) regime.

Accounting for both noise and DM-induced effects (Table II), the optical phase at the output of fiber i is

$$\phi_i = \underbrace{\phi_L}_{\substack{\text{input}\\\text{laser}\\\text{phase}}} - \omega_{0,L}\tau_{0,i}\left(\underbrace{1}_{\substack{\text{DC term}}} + \underbrace{\epsilon_{nx,i}\frac{\delta x}{x_0}}_{\substack{\text{DM-index}\\\text{coupling}}} + \underbrace{\epsilon_{n\omega_L,i}\frac{\delta\omega_L}{\omega_{0,L}}}_{\substack{\text{optical}\\\text{dispersion}}} + \underbrace{\epsilon_{Lx,i}\frac{\delta x}{x_0}}_{\substack{\text{DM-length}\\\text{coupling}}} + \underbrace{(1+\epsilon_{nL,i})h_i^{\text{acoustic}}}_{\substack{\text{mechanical}\\\text{vibrations}}} + \underbrace{\frac{\delta\omega_L}{\omega_{0,L}}}_{\substack{\text{laser frequency}\\\text{fluctuations}}}\right) + \underbrace{\delta\phi_i^{\text{thermal}}}_{\substack{\text{fiber thermal}\\\text{fluctuations}}}. \quad \text{(C2)}$$

3. Laser stabilized to fiber B

For this analysis, the schematic in Fig. 4 is assumed (see Appendix D 1), where fiber B acts as a delay line for stabilizing the laser. The inferred phase difference at

Photodetector B is $\Delta\Phi_B = \phi_L - \phi_B + \delta\phi_B^{\text{shot}}$, where ϕ_B^{shot} is the apparent phase imparted by shot noise. Stabilization can be achieved by tuning the laser's frequency using feedback based on the optical power measured by
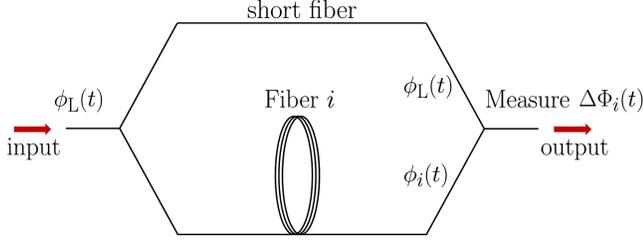
FIG. 5. Illustration of fiber interferometer, with relevant phases marked. The inferred output phase difference $\Delta\Phi_i(t) = \phi_L(t) - \phi_i(t) + \delta\phi_i^{\text{shot}}$ is determined by measuring the output optical power.

Photodetector B. For example, the laser's frequency can be tuned such that $\Delta\Phi_B \bmod 2\pi = \pi/2$, maintaining quadrature bias between the recombining beams before Photodetector B. At quadrature bias, where the output optical power depends linearly on the phase difference Φ_B, it can be shown [using Eq. (C2)] that the laser frequency fluctuations will be

$$\frac{\delta\omega_L}{\omega_{0,L}} = (1 + \epsilon_{n\omega_L,B})^{-1} \left(\frac{\frac{\pi}{2} + \delta\phi_B^{\text{thermal}} - \delta\phi_B^{\text{shot}}}{\omega_{0,L}\tau_{0,B}} \right.$$
$$\left. - (1 + \epsilon_{nL,B})h_B^{\text{acoustic}} - (\epsilon_{nx,B} - 1)\frac{\delta x}{x_0} \right). \quad \text{(C3)}$$

4. Detector output phase difference $\Delta\Phi_A$

The experimental observable in this experiment is the differential phase $\Delta\Phi_A$ between the output of fiber A and the interferometer's short arm, which is inferred from the measured optical power at Photodetector A. Here it is assumed that quadrature bias is maintained between the recombining beams before Photodetector A, which can be accomplished with a phase modulator that is driven by feedback from the power measured at Photodetector A. The DM signal would then be present in the feedback signal supplied to the modulator.

The phase difference $\Delta\Phi_A$ can be calculated using Eqs. (C2) and (C3). Ignoring zero-frequency terms, $\Delta\Phi_A$ is the sum of individual contributions from DM effects and each noise source

$$\Delta\Phi_A = \Delta\Phi_A^{\text{DM}} + \Delta\Phi_A^{\text{thermal}} + \Delta\Phi_A^{\text{acoustic}} + \Delta\Phi_A^{\text{shot}}.$$

Noting that $\epsilon_{nx} \sim \epsilon_{n\omega_L} \approx 10^{-2}$ and ignoring higher-order terms, it can be shown that

$$\Delta\Phi_A^{\text{DM}} \approx \omega_{0,L}\tau_0(\Delta\epsilon_{nx} + \Delta\epsilon_{n\omega_L})\frac{\delta x}{x_0} \quad \text{(C4)}$$

$$\Delta\Phi_A^{\text{acoustic}} \approx \omega_{0,L}\tau_0[(1 + \epsilon_{nL,A})h_A^{\text{acoustic}}$$
$$- (1 + \Delta\epsilon_{n\omega_L} + \epsilon_{nL,B})h_B^{\text{acoustic}}] \quad \text{(C5)}$$

$$\Delta\Phi_A^{\text{thermal}} \approx -\delta\phi_A^{\text{thermal}} + \delta\phi_B^{\text{thermal}} \quad \text{(C6)}$$

$$\Delta\Phi_A^{\text{shot}} \approx \delta\phi_A^{\text{shot}} - \delta\phi_B^{\text{shot}}, \quad \text{(C7)}$$

where we have assumed both fibers to have equal optical path lengths $\tau_{0,i} \equiv \tau_0$ for simplicity.

APPENDIX D: NOISE ANALYSIS

In this section we discuss the potential sources of noise that would act to obscure the DM-induced phase difference. The effect of each noise source is quantified by a one-sided phase noise PSD $S_{\Delta\Phi,A}(f)$.

1. Laser noise

Interferometric experiments are subject to noise from the driving laser, due to random fluctuations in the optical phase/frequency and intensity. Laser phase/frequency noise is eliminated in a perfectly balanced interferometer. However, when each arm is composed of different types of fiber with different levels of optical dispersion, an interferometer cannot remain balanced for all optical frequencies, and laser frequency noise is non-negligible. For the sensitivity of a balanced interferometer to reach the thermal noise floor at 50 mK, laser frequency noise needs to be limited to roughly $\sim 10^{-1}$ $(\text{Hz}/f)^{1/2}$ $\text{Hz} \cdot \text{Hz}^{-1/2}$; this would require an ultrastable laser [55].

Alternatively, laser frequency noise can be mitigated by stabilizing the frequency-tunable laser to one of the fibers, which acts as a delay line in a Mach-Zehnder interferometer. As a result, the laser's frequency noise PSD takes the form of the fiber delay line's (FDL)[1] phase noise PSD[2]: $S_{\delta\nu,L} = (2\pi\tau_0)^{-2}S_{\delta\phi,\text{FDL}}$ [56]. This procedure effectively eliminates laser frequency noise from the analysis, replacing it with phase noise from fiber B (which would have been present to the same level in a balanced interferometer).

For the detector depicted in Fig. 4, the "observable" is the phase difference $\Delta\Phi_A$ between the recombining optical paths before Photodetector A, which would still be affected by DM-induced modulation of the fiber refractive indices. At low frequencies ($f_{\text{DM}} \ll \tau_0^{-1}$), this is simply $\Delta\Phi_A = 2\pi n_A L_A/\lambda_L$ (prior to receiving corrections from the phase modulator). Because the laser is stabilized to fiber B, the laser wavelength is proportional to the optical path length of fiber B: $\lambda_L \propto n_B L_B$. Therefore, the detector's function is to compare the optical path lengths of fibers A and B, as $\Delta\Phi_A$ is

---

[1]Ultrastable lasers have been demonstrated using FDL stabilization. For example, a linewidth of 200 mHz has been achieved with a 5 km FDL at room temperature [36].

[2]This relationship holds for low frequencies, as the bandwidth of the control loop is limited by the time delay in the FDL [56]: $f \ll \tau_0^{-1} \approx 20$ kHz.

proportional to the ratio $n_A L_A / n_B L_B$. The balanced interferometer displayed in Fig. 1 is still a reasonable conceptual model for the detector, and it can be seen from the derivation for $\Delta\Phi_A$ in Appendix C the magnitude of the DM signal $\Delta\Phi^{DM}$ is unchanged in Eq. (6).

In addition to laser frequency noise, random fluctuations of the laser's optical intensity would limit the sensitivity of a detector like that depicted in Fig. 4. Experiments for measuring thermal noise in fibers have successfully minimized laser intensity noise to below the thermal noise floor with methods such as heterodyne detection [35] or with the use of differential amplifiers [34]. Assuming these methods are implemented, laser intensity noise is neglected in this analysis.

We note that the resulting appearance of the detector in Fig. 4 is similar to that of the DAMNED experiment [13] for scalar UDM, where an ultrastable laser drives an unbalanced fiber interferometer. There are, however, some key differences. While the detector we propose is sensitive to DM-induced refractive index modulation at sub-Hz frequencies, the DAMNED experiment is primarily sensitive to the DM-induced strain at kHz frequencies where their optical cavity has acoustic resonances. Schematically, the only major difference is the use of an optical fiber for stabilizing the laser instead of an ultrastable optical cavity. However, this distinction is important for suppressing acoustic noise at low frequencies (explained in Section D 4) to reach the fibers' thermal noise floor. By achieving a thermally limited measurement scheme, the sensitivity of the detector can then be enhanced through cryogenic cooling. In fact, operating at low temperatures will likely be necessary to set novel constraints on scalar UDM at sub-Hz frequencies, as demonstrated by the results in Fig. 3.

2. Photon shot noise and optical power

The phase difference $\Delta\Phi$ between the arms of an interferometer is inferred by measuring the output optical power P after the junction where the arms recombine. Assuming that the recombining beams have equal optical power and are maintained at quadrature bias,[3] the PSDs of the phase difference and output optical power fluctuations ΔP are related by $S_{\Delta\Phi} = S_{\Delta P}/\langle P \rangle^2$, where $\langle P \rangle$ is the average output optical power.

Small fluctuations in the measured optical power due to shot noise are indistinguishable from small phase fluctuations in an interferometer, thereby limiting the sensitivity of our setup. The one-sided PSD of the fluctuations in measured optical power due to shot noise is [57]

---

[3]At quadrature bias, the average phase difference between recombining beams at an interferometer's output is $\langle \Delta\Phi \rangle$ mod $2\pi = \pi/2$.

$$S_{\Delta P}^{shot} = \frac{2hc}{\lambda_{0,L}} \langle P \rangle. \tag{D1}$$

Assuming that the optical power imminent on each photodetector is equal,

$$\langle P \rangle = \frac{P_L}{2 + 10^{\gamma_B L_B} + 10^{\gamma_A L_A}}, \tag{D2}$$

where γ_i is the optical loss of fiber i and P_L is the optical power of the laser. The total contribution of shot noise to the differential phase noise of the detector is thus

$$S_{\Delta\Phi,A}^{shot} = \frac{4hc}{\lambda_{0,L}P_L}(2 + 10^{\gamma_B L_B} + 10^{\gamma_A L_A}), \tag{D3}$$

which is simply double the shot noise at each detector.

The effects of shot noise can be reduced by increasing the optical power. Figure 2 shows that a detector with bare fibers, operating at $T = 50$ mK, achieves a noise floor (combined thermomechanical and acoustic noise) of $\gtrsim 10^{-7}$ rad/$\sqrt{\text{Hz}}$. Reducing the total shot noise in this experiment to the subdominant level of $\sqrt{S_{\Delta\Phi,A}^{shot}} \lesssim 10^{-7}$ rad/$\sqrt{\text{Hz}}$ requires an average optical power on each photodetector of $\langle P \rangle \gtrsim 50$ μW.

Recent advances in hollow core fiber technology have yielded hollow core fibers with a propagation loss of 0.17 dB/km ($\gamma = 1.7 \times 10^{-5}$ m^{-1}) at $\lambda_{0,L} = 1550$ nm [39], reaching the level of low-loss solid core fibers (0.18 dB/km for SMF28 [40]), and we use these numbers for our shot noise estimates. In Fig. 2, the total shot noise is plotted for a detector with a 10 km solid core and ~15 km hollow core fiber, assuming a laser power of $P_L = 1$ mW. To account for optical loss, the optical power being diverted into the solid and hollow core fibers is taken to be 0.25 mW and 0.42 mW, respectively, and the power reaching each photodetector, $\langle P \rangle = 0.16$ mW.

3. Thermal noise in fibers

The detector's noise floor in the $10^{-3} - 10^1$ Hz frequency range will likely be dominated by thermal noise in the optical fibers, which will induce optical phase fluctuations $\delta\phi$ at the fiber outputs. Thermal noise in fibers includes contributions from two effects, which are referred to as "thermomechanical" noise $S_{\delta\phi}^{TM}$ (discussed in the main text) and "thermoconductive" noise $S_{\delta\phi}^{TC}$ [32]. Thermoconductive noise results from spontaneous local temperature fluctuations within an optical fiber [58,59] that affect the fiber's length and refractive index via thermal expansion and the thermo-optic effect, respectively [32]. We have estimated $S_{\delta\phi}^{TC}$ in solid core fibers using the parameters (for SMF28) and Eq. (1) from Ref. [35]. Thermoconductive noise in hollow core fibers

TABLE III. Parameters used for room temperature optical fibers with coatings. The solid core fiber is assumed to be SMF28 [40], and the hollow core fiber is assumed to be nested antiresonant nodeless fiber [62]. We also discuss how the parameters are affected by removing the fiber coatings and operating at cryogenic temperatures.

Quantity	Variable [Units]	Solid core	Hollow core
Refractive index	n_0 [-]	1.47 [40]	1
Optical loss	γ [m^{-1}]	1.8×10^{-5} [40]	2.8×10^{-5} [62]
Optical dispersion	$\epsilon_{n\omega_L}$ [-]	0.013 [54]	0
Stress-optic effect	ϵ_{nL} [-]	−0.17 [63]	0
Mechanical loss tangent	ξ [-]	10^{-2} [35,64]	10^{-2}[a]
Diameter of coating	d_{coat} [μm]	242 [40]	302[a]
Diameter of cladding	d_{clad} [μm]	125 [40]	185 [27]
Diameter of photonic crystal region	d_{pc} [μm]	0	70 [27]
Total cross sectional area	A [μm^2]	4.6×10^4	6.8×10^4
Young's modulus	E [GPa]	20	25

[a]The loss tangent and coating thickness for hollow core fiber is assumed equal to those of SMF28.

will likely be lower than that of solid core fibers at lower frequencies ($\lesssim 1$ kHz), especially in hollow core fibers that are evacuated [60].

Assuming the thermal noise for each fiber is uncorrelated,

$$S_{\Delta\Phi,A}^{\mathrm{thermal}} = \sum_i S_{\delta\phi,i}^{\mathrm{TM}} + S_{\delta\phi,i}^{\mathrm{TC}}. \tag{D4}$$

Thermoconductive noise is approximately frequency independent at lower frequencies ($\lesssim 1$ kHz), and scales with temperature and fiber length as $S_{\delta\phi}^{\mathrm{TC}} \propto T^2 L$ [61]. Thermomechanical noise, scaling as $S_{\delta\phi}^{\mathrm{TM}} \propto TL/f$, is expected to dominate the experiment given lower frequencies and temperatures considered here. This can be seen in the thermal noise curves in Fig. 2, which inherit the $1/f$ frequency scaling from thermomechanical noise, except for the 300 K bare case, where thermoconductive noise dominates above $\sim 10^{-2}$ Hz.

Key parameters for evaluating fiber thermomechanical noise using Eq. (7) are summarized in Table III. While the physical properties ξ and E have not been measured specifically for SMF28 fibers, the estimates found in Table III have been shown to reliably predict thermomechanical noise in SMF28 fibers [35] via Eq. (7). Below we provide details for the evaluation of E, and the choice of ξ for various scenarios considered in this work.

a. Young's modulus evaluation

The Young's modulus (E) is approximated for a fiber by a weighted average of the Young's moduli of each material over the cross sectional area [64]

$$E \approx \frac{A_{\mathrm{coat}} E_{\mathrm{coat}} + A_{\mathrm{clad}} E_{\mathrm{clad}}}{A}. \tag{D5}$$

The values $E_{\mathrm{clad}} = 66.1$ GPa for a silica fiber and $E_{\mathrm{coat}} = 3.3$ GPa for the polymer coating (assuming acrylate)

are used, based on measurements at kHz frequencies [64]. The Young's moduli are assumed to be frequency independent. The values for E in Table III are calculated from Eq. (D5) with the following cross sectional areas:

$$A \approx \frac{\pi}{4}(d_{\mathrm{coat}}{}^2 - d_{\mathrm{pc}}{}^2)$$

$$A_{\mathrm{coat}} = \frac{\pi}{4}(d_{\mathrm{coat}}{}^2 - d_{\mathrm{clad}}{}^2)$$

$$A_{\mathrm{clad}} \approx \frac{\pi}{4}(d_{\mathrm{clad}}{}^2 - d_{\mathrm{pc}}{}^2),$$

which approximate the hollow and photonic crystal regions to be empty space.

b. Bare fiber parameters

While fused silica optical fibers with a polymer coating have a loss tangent $\xi \approx 10^{-2}$ [35,64], bulk fused silica can potentially achieve $\xi \approx 10^{-8}$ at room temperature [65]. In addition, mechanical dissipation in the violin modes (transverse oscillations) of bare fibers at room temperature is typically around $\xi \approx 10^{-7}$–10^{-6} [66–68]. Noting that mechanical loss in a spooled optical fiber will likely differ from that of bulk silica or violin modes in silica suspensions under tension, a value of $\xi = 10^{-6}$ is assumed for bare fibers at room temperature. By setting $d_{\mathrm{coat}} = d_{\mathrm{clad}}$ the fibers' cross sectional areas and effective Young's moduli are recalculated, with all other parameters in Table III unchanged.

c. Low-temperature parameters

Measurements of the temperature dependence of the Young's modulus of fused silica [69] and the refractive index of fused silica fibers [70] suggest that n_0 and E_{clad} can be assumed constant with respect to temperature without appreciably affecting the estimates in Fig. 2. We assume

$\xi = 10^{-3}$ for cryogenic (50 mK) bare fibers, based on measurements in Ref. [71].

At low temperatures ($\sim$200 K), the acrylate coatings transition from a rubbery state to a stiffer, glassy state with a Young's modulus $E_{\text{coat}} \approx 40$ GPa [72], and the effective Young's modulus has been adjusted for coated fibers at 50 mK accordingly with Eq. (D5). However, due to the absence of data on mechanical dissipation in optical fibers at low temperatures, we assume $\xi = 10^{-2}$ for coated fibers at all temperatures.

4. Acoustic noise in fibers

Mechanical vibrations alter the optical path lengths of fibers, resulting in phase noise. Here we estimate the amplitude of mechanical vibrations, which we will generically refer to as "acoustic noise," and discuss techniques to potentially reduce the resulting phase noise to a subdominant level.

To estimate the effects of mechanical vibrations, we use the United States Geological Survey NHNM for seismic noise, which can be found in Table 4 in Ref. [38]. The NHNM provides an estimate of seismic acceleration noise S_{aa}^{seismic} for a hypothetical, relatively noisy location on Earth. For the frequency range considered in this work ($\sim 10^{-3} - 10^1$ Hz), the NHNM roughly predicts an upper bound of

$$S_{aa}^{\text{seismic}} \lesssim 10^{-9} \left(\frac{\text{m}}{\text{s}^2}\right)^2 \text{Hz}^{-1}, \qquad \text{(D6)}$$

which we extrapolate to frequencies above 10 Hz by assuming white acceleration noise $\sim 10^{-9} \left(\frac{\text{m}}{\text{s}^2}\right)^2 \text{Hz}^{-1}$. We will assume this seismic noise accounts for all of the vibrations the fibers will experience: $S_{aa}^{\text{acoustic}} \approx S_{aa}^{\text{seismic}}$.

Vibration-induced strains in optical fibers can be suppressed by using low vibration sensitivity fiber spools, a technology designed to reduce frequency noise in FDL-stabilized lasers [37]. This technique has been shown to produce ultrastable lasers at room temperature, reaching the thermomechanical noise floor in km-scale fibers at sub-Hz frequencies [36]. Such vibration-insensitive fiber spools have achieved sensitivities $\Gamma_a \equiv h^{\text{acoustic}}/a^{\text{acoustic}} \lesssim 10^{-11}$ (m/s^2)$^{-1}$ to both horizontal and vertical accelerations [73]. Thus, we expect acoustic noise to induce a strain noise in each fiber on the order of

$$S_{hh}^{\text{acoustic}} = |\Gamma_a|^2 S_{aa}^{\text{acoustic}} \lesssim 10^{-31} \text{ Hz}^{-1}. \qquad \text{(D7)}$$

In solid core fiber, this will lead to a change in the refractive index via the strain-optic effect

$$\frac{\delta n}{n_0} = \epsilon_{nL} h^{\text{acoustic}}. \qquad \text{(D8)}$$

From the analysis in Ref. [63], which considers a linear strain along a single mode fiber, it can be shown that $\epsilon_{nL,\text{solid}} \approx -0.17$.

Accounting for the strain-optic effect $\epsilon_{nL,i}$ and differences in optical dispersion $\Delta\epsilon_{n\omega_L}$, it can be shown that the output phase difference due to strains h_i^{acoustic} in both fibers is (see Appendix C)

$$\begin{aligned} \Delta\Phi_A^{\text{acoustic}} \approx \omega_{0,L}\tau_0[&(1+\epsilon_{nL,A})h_A^{\text{acoustic}} \\ &- \times(1+\Delta\epsilon_{n\omega_L}+\epsilon_{nL,B})h_B^{\text{acoustic}}]. \quad \text{(D9)} \end{aligned}$$

The strain-optic effect has a larger impact on the acoustic phase noise than the optical dispersion effect ($|\Delta\epsilon_{nL}| > |\Delta\epsilon_{n\omega_L}|$).

If the individual fiber strains are correlated and of equal magnitude $h_A^{\text{acoustic}} = h_B^{\text{acoustic}}$,

$$S_{\Delta\Phi,A}^{\text{acoustic}} = |\omega_{0,L}\tau_0(\Delta\epsilon_{n\omega_L}+\Delta\epsilon_{nL})|^2 S_{hh}^{\text{acoustic}}. \qquad \text{(D10)}$$

This can be accomplished by cowinding the fibers on a spool or cylinder, a technique that has been used to observe the thermal noise floor in fiber-based interferometers [34,35]. By cowinding both fibers on a single spool with $\Gamma_a \lesssim 10^{-11}$ (m/s^2)$^{-1}$, acoustic noise at the level predicted by the NHNM can be reduced to a level comparable to that of thermal noise in this experiment, as can be seen in Fig. 2. If desired, further suppression of vibration-induced phase noise can also be achieved using the feedforward method [74,75].

Appendix E: MINIMUM DETECTABLE SIGNAL VS MEASUREMENT TIME

The purpose of this Appendix is to motivate Eq. (8), which describes how the minimum detectable signal $\Delta\Phi_{\text{min}}^{\text{DM}}$ scales with the measurement time τ_{exp}. There are two separate regimes for dark matter detection, the "stochastic" ($\tau_{\text{exp}} \lesssim \tau_{\text{DM}}$) and "deterministic" ($\tau_{\text{exp}} \gg \tau_{\text{DM}}$) regimes [20]. As discussed in Ref. [42], $\Delta\Phi_{\text{min}}^{\text{DM}} \propto \tau_{\text{exp}}^{-1/2}$ for a coherent signal and $\Delta\Phi_{\text{min}}^{\text{DM}} \propto \tau_{\text{exp}}^{-1/4}$ for measurement durations greatly exceeding the DM coherence time. Here we provide a complementary analysis using a discrete Fourier transform (DFT) formalism and join both regimes with a single expression for the DM-induced phase difference.

We consider the case where the measurement is contaminated by noise $\Delta\Phi^{\text{noise}}$. Performing a measurement of duration τ_{exp} with a sampling rate of f_s, a periodogram $S_{\Delta\Phi,k}^{\text{noise}}$ can be obtained from the DFT $\Delta\tilde{\Phi}_k^{\text{noise}}$ as $S_{\Delta\Phi,k}^{\text{noise}} = 2|\Delta\tilde{\Phi}_k^{\text{noise}}|^2/Nf_s$, where $N \equiv f_s\tau_{\text{exp}}$. Here, the subscript k refers to the bin number. Assuming Gaussian noise, the periodogram's standard deviation can be approximated by its mean [76], which for a broadband noise source can be estimated simply by sampling the PSD: $\langle S_{\Delta\Phi,k}^{\text{noise}}\rangle \approx S_{\Delta\Phi}^{\text{noise}}(kf_s/N)$. This expression is valid in the large N limit.

Here we define the minimum detectable signal strength $\Delta\Phi_{\min}^{\mathrm{DM}}$ as the signal amplitude required for the signal power to equal the variance in the noise floor, i.e.

$$S_{\Delta\Phi,k}^{\mathrm{DM}} = S_{\Delta\Phi}^{\mathrm{noise}}(kf_s/N). \tag{E1}$$

In the following sections we explore the relationship between $\Delta\Phi_{\min}^{\mathrm{DM}}$ and the expected noise floor $S_{\Delta\Phi}^{\mathrm{noise}}(kf_s/N)$ for the stochastic and deterministic regimes.

1. Minimum detectable signal for $\tau_{\mathrm{exp}} \lesssim \tau_{\mathrm{DM}}$

For measurement times less than the DM coherence time the signal is approximately coherent $\Delta\Phi^{\mathrm{DM}} \approx \Delta\Phi_0^{\mathrm{DM}} \times \cos(2\pi f_{\mathrm{DM}}t + \theta_{\mathrm{DM}})$. For a coherent signal, the signal power is entirely contained within a single frequency bin,

$$S_{\Delta\Phi,k}^{\mathrm{DM}} = \frac{1}{2}(\Delta\Phi_0^{\mathrm{DM}})^2 \tau_{\mathrm{exp}}. \tag{E2}$$

From Eq. (E1), the minimum detectable signal would be $\Delta\Phi_{\min}^{\mathrm{DM}} \approx \sqrt{2S_{\Delta\Phi}^{\mathrm{noise}}}\tau_{\mathrm{exp}}^{-1/2}$.

This analysis so far assumed a deterministic signal amplitude $\Delta\Phi_0^{\mathrm{DM}}$. However, due to interference of UDM field components of differing frequency and phase, the field's amplitude fluctuates over timescales roughly equal to τ_{DM}. The field amplitude within a chunk of time τ_{DM}, φ_0, is a stochastic quantity with a Rayleigh distribution, where $\sim 63\%$ of all realizations are less than φ_{rms}, resulting in a reduced signal [20]. Therefore, a DM signal in the stochastic regime would need an amplitude ~ 3 times larger than an otherwise identical signal with deterministic amplitude to have the same probability of detection [20]. Accounting for the stochastic nature of the UDM field, the minimum detectable signal is

$$\Delta\Phi_{\min}^{\mathrm{DM}} \approx 3\sqrt{2S_{\Delta\Phi}^{\mathrm{noise}}}\tau_{\mathrm{exp}}^{-1/2}. \tag{E3}$$

2. Minimum detectable signal for $\tau_{\mathrm{exp}} \gg \tau_{\mathrm{DM}}$

For measurement times exceeding the DM coherence time, the signal power would be spread across $\sim \tau_{\mathrm{exp}}/\tau_{\mathrm{DM}}$ frequency bins. However, the measurement could be split into $M = \tau_{\mathrm{exp}}/\tau_{\mathrm{DM}}$ shorter measurements of duration τ_{DM}. This procedure is known as Bartlett's method (described in Ref. [76]), where the total periodogram would be the average of the M short-time periodograms, resulting in an M-fold reduction in the variance in the noise floor $S_{\Delta\Phi}^{\mathrm{noise}} \to S_{\Delta\Phi}^{\mathrm{noise}}/\sqrt{M}$. Each individual data segment is duration τ_{DM}, so $S_{\Delta\Phi,k}^{\mathrm{DM}} \approx (\Delta\Phi_0^{\mathrm{DM}})^2\tau_{\mathrm{DM}}/2$. The minimum detectable signal amplitude is then
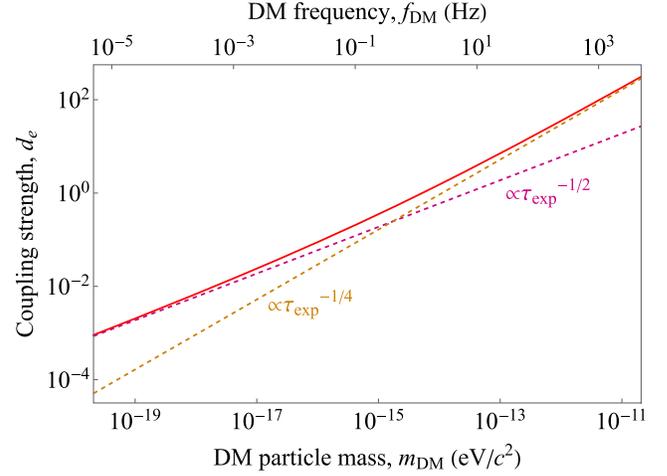
FIG. 6. Dependence of $d_{e,\min}$ on τ_{exp}. We approximate the minimum detectable signal strength's dependence on the total measurement time with Eq. (8) [Eq. (E5)], which accounts for both measurement regimes: $\tau_{\mathrm{exp}} \lesssim \tau_{\mathrm{DM}}$ (where $\Delta\Phi_{\min}^{\mathrm{DM}} \propto \tau_{\mathrm{exp}}^{-1/2}$) and $\tau_{\mathrm{exp}} \gg \tau_{\mathrm{DM}}$ (where $\Delta\Phi_{\min}^{\mathrm{DM}} \propto \tau_{\mathrm{exp}}^{-1/4}$). Here, $d_{e,\min}$ is calculated using Eq. (E3) (dashed pink line), Eq. (E4) (dashed yellow line), and Eq. (E5) (red curve), assuming a noise floor limited purely by the thermomechanical noise of room temperature, coated fibers. It can be seen that the combined expression from Eq. (E5) converges to the $\propto \tau_{\mathrm{exp}}^{-1/2}$ and $\propto \tau_{\mathrm{exp}}^{-1/4}$ limits at low and high frequencies, respectively.

$$\Delta\Phi_{\min}^{\mathrm{DM}} \approx \sqrt{2S_{\Delta\Phi}^{\mathrm{noise}}}(\tau_{\mathrm{DM}}\tau_{\mathrm{exp}})^{-1/4}. \tag{E4}$$

3. Combined expression for $\Delta\Phi_{\min}^{\mathrm{DM}}$

For measurement times less than the DM coherence time, the minimum detectable signal scales as $\propto \tau_{\mathrm{exp}}^{-1/2}$ [Eq. (E3)]. For measurement times greatly exceeding the DM coherence time, the minimum detectable signal scales as $\propto \tau_{\mathrm{exp}}^{-1/4}$ [Eq. (E4)]. This relationship between $\Delta\Phi_{\min}^{\mathrm{DM}}$ and τ_{exp} is a broken power law, which we simplify with a "smoothly joined broken power law" [77] by simply adding contributions from both regimes as

$$\Delta\Phi_{\min}^{\mathrm{DM}} \approx \sqrt{2S_{\Delta\Phi}^{\mathrm{noise}}}[3\tau_{\mathrm{exp}}^{-1/2} + (\tau_{\mathrm{DM}}\tau_{\mathrm{exp}})^{-1/4}]. \tag{E5}$$

This function reproduces the behavior of Eqs. (E3) and (E4) in the limits $\tau_{\mathrm{exp}} \ll \tau_{\mathrm{DM}}$ and $\tau_{\mathrm{exp}} \gg \tau_{\mathrm{DM}}$, respectively, while resulting in a larger $\Delta\Phi_{\min}^{\mathrm{DM}}$ in the $\tau_{\mathrm{exp}} \approx \tau_{\mathrm{DM}}$ regime, as shown in Fig. 6. This effect is desirable, as there would be some carryover of stochastic effects in this regime.

[1] P. A. Zyla, R. M. Barnett, J. Beringer, O. Dahl, D. A. Dwyer, D. E. Groom, C.-J. Lin, K. S. Lugovsky, E. Pianori *et al.* (Particle Data Group), Review of particle physics, Prog. Theor. Exp. Phys. **2020,** 083C01 (2020).

[2] Marco Battaglieri, Alberto Belloni, Aaron Chou, Priscilla Cushman, Bertrand Echenard, Rouven Essig, Juan Estrada, Jonathan L. Feng, Brenna Flaugher, Patrick J. Fox *et al.*, Us cosmic visions: New ideas in dark matter 2017: Community report, arXiv:1707.04591.

[3] D. Antypas, A. Banerjee, C. Bartram, M. Baryakhtar, J. Betz, J. J. Bollinger, C. Boutan, D. Bowring, D. Budker, D. Carney *et al.*, New horizons: Scalar and vector ultralight dark matter, arXiv:2203.14915.

[4] Thibault Damour and Alexander M. Polyakov, The string dilation and a least coupling principle, Nucl. Phys. **B423,** 532 (1994).

[5] Ken Van Tilburg, Nathan Leefer, Lykourgos Bougas, and Dmitry Budker, Search for Ultralight Scalar Dark Matter with Atomic Spectroscopy, Phys. Rev. Lett. **115,** 011802 (2015).

[6] A. Hees, J. Guéna, Michel Abgrall, S. Bize, and P. Wolf, Searching for an Oscillating Massive Scalar Field as a Dark Matter Candidate Using Atomic Hyperfine Frequency Comparisons, Phys. Rev. Lett. **117,** 061301 (2016).

[7] Kyle Beloy and Martha I. Bodine, Frequency ratio measurements at 18-digit accuracy using an optical clock network, Nature (London) **591,** 564 (2021).

[8] M. Filzinger, S. Dörscher, R. Lange, J. Klose, M. Steinel, E. Benkler, E. Peik, C. Lisdat, and N. Huntemann, Improved Limits on the Coupling of Ultralight Bosonic Dark Matter to Photons from Optical Atomic Clock Comparisons, Phys. Rev. Lett. **130,** 253001 (2023).

[9] Nathaniel Sherrill, Adam O. Parsons, Charles F. A. Baynham, William Bowden, E. Anne Curtis, Richard Hendricks, Ian R. Hill, Richard Hobson, Helen S. Margolis, Billy I. Robertson *et al.*, Analysis of atomic-clock data to constrain variations of fundamental constants, arXiv:2302.04565.

[10] William M. Campbell, Ben T. McAllister, Maxim Goryachev, Eugene N. Ivanov, and Michael E. Tobar, Searching for Scalar Dark Matter via Coupling to Fundamental Constants with Photonic, Atomic, and Mechanical Oscillators, Phys. Rev. Lett. **126,** 071301 (2021).

[11] Andrew A. Geraci, Colin Bradley, Dongfeng Gao, Jonathan Weinstein, and Andrei Derevianko, Searching for Ultralight Dark Matter with Optical Cavities, Phys. Rev. Lett. **123,** 031304 (2019).

[12] Colin J. Kennedy, Eric Oelker, John M. Robinson, Tobias Bothwell, Dhruv Kedar, William R. Milner, G. Edward Marti, Andrei Derevianko, and Jun Ye, Precision Metrology Meets Cosmology: Improved Constraints on Ultralight Dark Matter from Atom-Cavity Frequency Comparisons, Phys. Rev. Lett. **125,** 201302 (2020).

[13] Etienne Savalle, Aurélien Hees, Florian Frank, Etienne Cantin, Paul-Eric Pottie, Benjamin M. Roberts, Lucie Cros, Ben T. McAllister, and Peter Wolf, Searching for Dark Matter with an Optical Cavity and an Unequal-Delay Interferometer, Phys. Rev. Lett. **126,** 051301 (2021).

[14] Asimina Arvanitaki, Junwu Huang, and Ken Van Tilburg, Searching for dilaton dark matter with atomic clocks, Phys. Rev. D **91,** 015015 (2015).

[15] Jack Manley, Dalziel J. Wilson, Russell Stump, Daniel Grin, and Swati Singh, Searching for Scalar Dark Matter with Compact Mechanical Resonators, Phys. Rev. Lett. **124,** 151301 (2020).

[16] Sander M. Vermeulen, Philip Relton, Hartmut Grote, Vivien Raymond, Christoph Affeldt, Fabio Bergamin, Aparna Bisht, Marc Brinkmann, Karsten Danzmann, Suresh Doravari *et al.*, Direct limits for scalar field dark matter from a gravitational-wave detector, Nature (London) **600,** 424 (2021).

[17] Lorenzo Aiello, Jonathan W. Richardson, Sander M. Vermeulen, Hartmut Grote, Craig Hogan, Ohkyung Kwon, and Chris Stoughton, Constraints on Scalar Field Dark Matter from Twin Co-Located Power-Recycled Michelson Interferometers, Phys. Rev. Lett. **128,** 121101 (2022).

[18] Antonio Branca, Michele Bonaldi, Massimo Cerdonio, Livia Conti, Paolo Falferi, Francesco Marin, Renato Mezzena, Antonello Ortolan, Giovanni A. Prodi, Luca Taffarello *et al.*, Search for an Ultralight Scalar Dark Matter Candidate with the Auriga Detector, Phys. Rev. Lett. **118,** 021302 (2017).

[19] Philip St J. Russell, Photonic-crystal fibers, J. Lightwave Technol. **24,** 4729 (2006).

[20] Gary P. Centers, John W. Blanchard, Jan Conrad, Nataniel L. Figueroa, Antoine Garcon, Alexander V. Gramolin, Derek F. Jackson Kimball, Matthew Lawson, Bart Pelssers, Joseph A. Smiga *et al.*, Stochastic fluctuations of bosonic dark matter, Nat. Commun. **12,** 7321 (2021).

[21] Andrei Derevianko, Detecting dark-matter waves with a network of precision-measurement tools, Phys. Rev. A **97,** 042506 (2018).

[22] Thibault Damour and John F. Donoghue, Equivalence principle violations and couplings of a light dilaton, Phys. Rev. D **82,** 084033 (2010).

[23] C. Braxmaier, O. Pradl, H. Müller, A. Peters, J. Mlynek, V. Loriette, and S. Schiller, Proposed test of the time independence of the fundamental constants α and m e/m p using monolithic resonators, Phys. Rev. D **64,** 042001 (2001).

[24] Y. V. Stadnik and V. V. Flambaum, Searching for Dark Matter and Variation of Fundamental Constants with Laser and Maser Interferometry, Phys. Rev. Lett. **114,** 161301 (2015).

[25] Asimina Arvanitaki, Savas Dimopoulos, and Ken Van Tilburg, Sound of Dark Matter: Searching for Light Scalars with Resonant-Mass Detectors, Phys. Rev. Lett. **116,** 031102 (2016).

[26] Hartmut Grote and Y. V. Stadnik, Novel signatures of dark matter in laser-interferometric gravitational-wave detectors, Phys. Rev. Res. **1,** 033187 (2019).

[27] Bo Shi, Hesham Sakr, John Hayes, Xuhao Wei, Eric Numkam Fokoua, Meng Ding, Zitong Feng, Giuseppe Marra, Francesco Poletti, David J. Richardson *et al.*, Thinly coated hollow core fiber for improved thermal phase-stability performance, Opt. Lett. **46,** 5177 (2021).

[28] T. D. Bradley, *et al.*, Antiresonant hollow core fibre with 0.65 dB/km attenuation across the C and L telecommunication bands, in *Proceedings of the 45th European Conference on Optical Communication (ECOC 2019), Dublin, Ireland, 2019* (IET, IEEE, 2019), pp. 1–4, https://doi.org/10.1049/cp.2019.1028.

[29] Gregory T. Jasion, Thomas D. Bradley, Kerrianne Harrington, Hesham Sakr, Yong Chen, Eric Numkam Fokoua, Ian A. Davidson, Austin Taranta, John R. Hayes, David J. Richardson *et al.*, Recent breakthroughs in hollow core fiber technology, in *Proceedings of the Optical Fiber Communication Conference* (Optical Society of America, Washington, DC, 2021), pp. M5E–2.

[30] Joel Bergé, Philippe Brax, Gilles Métris, Martin Pernot-Borràs, Pierre Touboul, and Jean-Philippe Uzan, Microscope Mission: First Constraints on the Violation of the Weak Equivalence Principle by a Light Scalar Dilaton, Phys. Rev. Lett. **120**, 141101 (2018).

[31] Lukáš F Pašteka, Yongliang Hao, Anastasia Borschevsky, Victor V. Flambaum, and Peter Schwerdtfeger, Material Size Dependence on Fundamental Constants, Phys. Rev. Lett. **122**, 160801 (2019).

[32] Lingze Duan, General treatment of the thermal noises in optical fibers, Phys. Rev. A **86**, 023817 (2012).

[33] L. Z. Duan, Intrinsic thermal noise of optical fibres due to mechanical dissipation, Electron. Lett. **46**, 1515 (2010).

[34] Robert E. Bartolo, Alan B. Tveten, and Anthony Dandridge, Thermal phase noise measurements in optical fiber interferometers, IEEE J. Quantum Electron. **48**, 720 (2012).

[35] Jing Dong, Junchao Huang, Tang Li, and Liang Liu, Observation of fundamental thermal noise in optical fibers down to infrasonic frequencies, Appl. Phys. Lett. **108**, 021108 (2016).

[36] Junchao Huang, Lingke Wang, Yifei Duan, Yafeng Huang, Meifeng Ye, Liang Liu, and Tang Li, All-fiber-based laser with 200 mHz linewidth, Chin. Optic. Lett. **17**, 071407 (2019).

[37] T. Li, B. Argence, A. Haboucha, H. Jiang, J. L. Dornaux, D. Koné, A. Clairon, P. Lemonde, G. Santarelli, C. Nelson *et al.*, Low vibration sensitivity fiber spools for laser stabilization, in *Proceedings of the 2011 Joint Conference of the IEEE International Frequency Control and the European Frequency and Time Forum (FCS) Proceedings* (IEEE, New York, 2011), pp. 1–3.

[38] Jon R. Peterson, Observations and modeling of seismic background noise, US Geological Survey Technical Report No. 93-322, 1993.

[39] Gregory T. Jasion, Hesham Sakr, John R. Hayes, Seyed Reza Sandoghchi, Lucy Hooper, Eric Numkam Fokoua, Arsalan Saljoghei, Hans Christian Mulvad, Marcelo Alonso, Austin Taranta *et al.*, 0.174 db/km hollow core double nested antiresonant nodeless fiber (DNANF), in *Proceedings of the 2022 Optical Fiber Communications Conference and Exhibition (OFC)* (IEEE, New York, 2022), pp. 1–3.

[40] Corning SMF-28 Ultra Optical Fiber Product Information, Corning, 2021, https://www.corning.com/optical-communications/worldwide/en/home/products/fiber/optical-fiber-products/smf-28-ultra.html.

[41] Christopher Hilweg, Danial Shadmany, Philip Walther, Nergis Mavalvala, and Vivishek Sudhir, Limits and prospects for long-baseline optical fiber interferometry, Optica **9**, 1238 (2022).

[42] Dmitry Budker, Peter W. Graham, Micah Ledbetter, Surjeet Rajendran, and Alexander O. Sushkov, Proposal for a Cosmic Axion Spin Precession Experiment (CASPER), Phys. Rev. X **4**, 021030 (2014).

[43] Abhishek Banerjee, Dmitry Budker, Joshua Eby, Hyungjin Kim, and Gilad Perez, Relaxion stars and their detection via atomic physics, Commun. Phys. **3**, 1 (2020).

[44] R. Oswald, A. Nevsky, V. Vogt, S. Schiller, N. L. Figueroa, K. Zhang, O. Tretiak, D. Antypas, D. Budker, A. Banerjee *et al.*, Search for Oscillations of Fundamental Constants Using Molecular Spectroscopy, Phys. Rev. Lett. **129**, 031302 (2022),

[45] D. Antypas, O. Tretiak, A. Garcon, R. Ozeri, G. Perez, and D. Budker, Scalar Dark Matter in the Radio-Frequency Band: Atomic-Spectroscopy Search Results, Phys. Rev. Lett. **123**, 141102 (2019).

[46] Shahaf Aharony, Nitzan Akerman, Roee Ozeri, Gilad Perez, Inbar Savoray, and Ravid Shaniv, Constraining rapidly oscillating scalar dark matter using dynamic decoupling, Phys. Rev. D **103**, 075017 (2021).

[47] Abhishek Banerjee, Dmitry Budker, Joshua Eby, Victor V. Flambaum, Hyungjin Kim, Oleksii Matsedonskyi, and Gilad Perez, Searching for earth/solar axion halos, J. High Energy Phys. 09 (2020) 004.

[48] Stephan Schlamminger, K.-Y. Choi, Todd A. Wagner, Jens H. Gundlach, and Eric G. Adelberger, Test of the Equivalence Principle Using a Rotating Torsion Balance, Phys. Rev. Lett. **100**, 041101 (2008).

[49] Daniel Carney, Anson Hook, Zhen Liu, Jacob M. Taylor, and Yue Zhao, Ultralight dark matter detection with mechanical quantum sensors, New J. Phys. **23**, 023041 (2021).

[50] P. Delva, J. Lodewyck, S. Bilicki, E. Bookjans, Guy Vallet, R. Le Targat, P.-E. Pottie, C. Guerlin, F. Meynadier, C. Le Poncin-Lafitte *et al.*, Test of Special Relativity Using a Fiber Network of Optical Clocks, Phys. Rev. Lett. **118**, 221102 (2017).

[51] Christian Lisdat, Gesine Grosche, N. Quintin, C. Shi, S. M. F. Raupach, C. Grebing, D. Nicolodi, F. Stefani, A. Al-Masoudi, S. Dörscher *et al.*, A clock network for geodesy and fundamental science, Nat. Commun. **7**, 12443 (2016).

[52] D. D. Yavuz and S. Inbar, Generation and detection of axions using guided structures, Phys. Rev. D **105**, 074012 (2022).

[53] Mikhail G. Kozlov and Dmitry Budker, Comment on sensitivity coefficients to variation of fundamental constants, Ann. Phys. (Berlin) **531**, 1800254 (2019).

[54] Ian H. Malitson, Interspecimen comparison of the refractive index of fused silica, J. Opt. Soc. Am. **55**, 1205 (1965).

[55] Lifei Wu, Yanyi Jiang, Chaoqun Ma, Wen Qi, Hongfu Yu, Zhiyi Bi, and Longsheng Ma, 0.26-Hz-linewidth ultrastable lasers at 1557 nm, Sci. Rep. **6**, 24969 (2016).

[56] Jing Dong, Yongqi Hu, Junchao Huang, Meifeng Ye, Qiuzhi Qu, Tang Li, and Liang Liu, Subhertz linewidth laser by locking to a fiber delay line, Appl. Opt. **54**, 1152 (2015).

[57] Aashish A. Clerk, Michel H. Devoret, Steven M. Girvin, Florian Marquardt, and Robert J. Schoelkopf, Introduction to quantum noise, measurement, and amplification, Rev. Mod. Phys. **82**, 1155 (2010).

[58] Charles Kittel, Temperature fluctuation: An oxymoron, Phys. Today **41**, No. 5, 93 (1988).

[59] William H. Glenn, Noise in interferometric optical systems: An optical Nyquist theorem, IEEE J. Quantum Electron. **25**, 1218 (1989).

[60] Vincent Michaud-Belleau, Eric R Numkam Fokoua, Peter Horak, Natalie V. Wheeler, Shuichiro Rikimi, Thomas D. Bradley, David J. Richardson, Francesco Poletti, Jérôme Genest, and Radan Slavík, Fundamental thermal noise in antiresonant hollow-core fibers, Phys. Rev. A **106**, 023501 (2022).

[61] K. H. Wanser, Fundamental phase noise limit in optical fibres due to temperature fluctuations, Electron. Lett. **28**, 53 (1992).

[62] Gregory T. Jasion, Thomas D. Bradley, Kerrianne Harrington, Hesham Sakr, Yong Chen, Eric Numkam Fokoua, Ian A. Davidson, Austin Taranta, John R. Hayes, David J. Richardson *et al.*, Hollow core nanf with 0.28 db/km attenuation in the c and l bands, in *Proceedings of the Optical Fiber Communication Conference* (Optical Society of America, San Diego, CA, 2020), pp. Th4B–4.

[63] Charles D. Butter and G. B. Hocker, Fiber optics strain gauge, Appl. Opt. **17**, 2867 (1978).

[64] Brad M. Beadle and Jacek Jarzynski, Measurement of speed and attenuation of longitudinal elastic waves in optical fibers, Opt. Eng. **40**, 2115 (2001).

[65] Anja Schroeter, Ronny Nawrodt, Roman Schnabel, Stuart Reid, Iain Martin, Sheila Rowan, Christian Schwarz, Torsten Koettig, Ralf Neubert, Matthias Thürk *et al.*, On the mechanical quality factors of cryogenic test masses from fused silica and crystalline quartz, arXiv:0709.4359.

[66] Andri M. Gretarsson and Gregory M. Harry, Dissipation of mechanical energy in fused silica fibers, Rev. Sci. Instrum. **70**, 4081 (1999).

[67] Steven D. Penn, Gregory M. Harry, Andri M. Gretarsson, Scott E. Kittelberger, Peter R. Saulson, John J. Schiller, Joshua R. Smith, and Sol O. Swords, High quality factor measured in fused silica, Rev. Sci. Instrum. **72**, 3670 (2001).

[68] Alastair Heptonstall, Mark Barton, Caroline Cantley, Alan Cumming, Geppo Cagnoli, James Hough, Russell Jones, Rahul Kumar, Iain Martin, Sheila Rowan *et al.*, Investigation of mechanical dissipation in co2 laser-drawn fused silica fibres and welds, Classical Quantum Gravity **27**, 035013 (2010).

[69] H. J. McSkimin, Measurement of elastic constants at low temperatures by means of ultrasonic waves–data for silicon and germanium single crystals, and for fused silica, J. Appl. Phys. **24**, 988 (1953).

[70] Max B. Reid and Meric Ozcan, Temperature dependence of fiber optic Bragg gratings at low temperatures, Opt. Eng. **37**, 237 (1998).

[71] R. O. Behunin, P. Kharel, W. H. Renninger, and P. T. Rakich, Engineering dissipation with phononic spectral hole burning, Nat. Mater. **16**, 315 (2017).

[72] Wenwu Zhu, Eric R. Numkam Fokoua, Austin A. Taranta, Yong Chen, Thomas Bradley, Marco N. Petrovich, Francesco Poletti, Mingshan Zhao, David J. Richardson, and Radan Slavík, The thermal phase sensitivity of both coated and uncoated standard and hollow core fibers down to cryogenic temperatures, J. Lightwave Technol. **38**, 2477 (2020).

[73] Junchao Huang, Lingke Wang, Yifei Duan, Yafeng Huang, Meifeng Ye, Lin Li, Liang Liu, and Tang Li, Vibration-insensitive fiber spool for laser stabilization, Chin. Optic. Lett. **17**, 081403 (2019).

[74] Michael J. Thorpe, David R. Leibrandt, Tara M. Fortier, and Till Rosenband, Measurement and real-time cancellation of vibration-induced phase noise in a cavity-stabilized laser, Opt. Express **18**, 18744 (2010).

[75] David R. Leibrandt, James C. Bergquist, and Till Rosenband, Cavity-stabilized laser with acceleration sensitivity below 10- 12 g- 1, Phys. Rev. A **87**, 023829 (2013).

[76] John G. Proakis and Dimitris K. Manolakis, *Digital Signal Processing (4th Edition)* (Prentice Hall, Englewood Cliffs, NJ, 2006), ISBN: 0131873741.

[77] K. Beuermann, F. V. Hessman, K. Reinsch, H. Nicklas, P. M. Vreeswijk, T. J. Galama, E. Rol, J. van Paradijs, C. Kouveliotou, F. Frontera, N. Masetti, E. Palazzi, and E. Pian, VLT observations of GRB 990510 and its environment, arXiv:astro-ph/9909043.